Inorg. Chem. **2005**, *44*, 862–874

Coordination Polymers Based on Inorganic Lanthanide(III) Sulfate Skeletons and an Organic Isonicotinate *N*-oxide Connector: Segregation into Three Structural Types by the Lanthanide Contraction Effect

Zheng He,[†] En-Qing Gao,[†,‡] Zhe-Ming Wang,*[,†] Chun-Hua Yan,*[,†] and Mohamedally Kurmoo[§]

State Key Lab of Rare Earth Materials Chemistry and Applications & PKU−HKU Joint Lab on Rare Earth Materials and Bioinorganic Chemistry, Peking University, Beijing 100871, China, Shanghai Key Lab of Green Chemistry and Chemical Processes, East-China Normal University, Shanghai 200062, China, and Laboratoire de Chimie de Coordination Organique, UMR7140−CNRS, Université Louis Pasteur, Institut Le Bel, 4 rue Blaise Pascal, 67000 Strasbourg Cedex, France

Fourteen three-dimensional coordination polymers of general formula $[Ln(INO)(H_2O)(SO_4)]_n$, where Ln = La, **1**·La; Ce, **2**·Ce; Pr, **3**·Pr; Nd, **4**·Nd; Sm, **5**·Sm; Eu, **6**·Eu; Gd, **7**·Gd; Tb, **8**·Tb; Dy, **9**·Dy; Ho, **10**·Ho; Er, **11**·Er; Tm, **12**·Tm; Yb, **13**·Yb; and Lu, **14**·Lu; INO = isonicotinate-*N*-oxide, have been synthesized by hydrothermal reactions of Ln^{3+}, $MnCO_3$, $MnSO_4 \cdot H_2O$, and isonicotinic acid *N*-oxide (HINO) at 155 °C and characterized by single-crystal X-ray diffraction, IR, thermal analysis, luminescence spectroscopy, and the magnetic measurement. The structures are formed by connection of layer, chain, or dimer of Ln–SO_4 by the organic connector, INO. They belong to three structural types that are governed exclusively by the size of the ions: type I for the large ions, La, Ce, and Pr; type II for the medium ions, Nd, Sm, Eu, Gd, and Tb; and type III for the small ions, Dy, Ho, Er, Tm, Yb, and Lu. Type I consists of two-dimensional undulate Ln–sulfate layers pillared by INO to form a three-dimensional network. Type II has a 2-fold interpenetration of "3D herringbone" networks, in which the catenation is sustained by extensive π–π interactions and O–H···O and C–H···O hydrogen bonds. Type III comprises one-dimensional chains that are connected by INO bridges, resulting in an α-Po network. The progressive structural change is due to the metal coordination number decreasing from nine for the large ions via eight to seven for the small ions, demonstrating clearly the effect of lanthanide contraction. The sulfate ion acts as a μ_4- or μ_3-bridge, connecting two, three, or four metals, and is both mono- and bidentate. The INO ligand acts as a μ_3- or μ_2-bridge with carboxylate group in syn–syn bridging or bidentate chelating mode. The materials show considerably high thermal stability. The magnetic properties of **4**·Nd, **6**·Eu, **7**·Gd, and **13**·Yb and the luminescence properties of **6**·Eu and **8**·Tb are also investigated.

Introduction

The rational design of coordination polymers with predictable structures has spurred great interest not only for their potential applications as functional materials (catalysts, chromatographic media, magnets, and nonlinear optics) but also for their intrinsic structural aesthetic appeal.[1] Consequently, a variety of coordination polymers with interesting compositions, d- and f-elements, neutral and charged organic ligands, as well as coordinating organic and inorganic anions, have been prepared through careful selection of the metal ion and the constituent ligands.[2] They present a wide range of topologies that have been very fruitful in realizing some of the frameworks proposed by Wells.[3] Most of these work have been focused on coordination polymers containing transition-metal ions but few lanthanide ions, because of the

* To whom correspondence should be addressed. Fax: +86-10-62754179. E-mail: yan@pku.edu.cn (C.-H.Y.), zmw@pku.edu.cn (Z.-M.W.).
[†] Peking University.
[‡] East-China Normal University.
[§] Université Louis Pasteur.

(1) (a) Moulton, B.; Zaworotko, M. J. *Chem. Rev.* **2001**, *101*, 1629. (b) Eddaoudi, M.; Moler, D. B.; Li, H.; Chen, B.; Reineke, T. M.; O'Keeffe, M.; Yaghi, O. M. *Acc. Chem. Res.* **2001**, *34*, 319.

(2) (a) Reger, D. L.; Wright, T. D.; Semeniuc, R. F.; Grattan, T. C.; Smith, M. D. *Inorg. Chem.* **2001**, *40*, 6212. (b) Kitaura, R.; Seki, K.; Akiyama, G.; Kitagawa, S. *Angew. Chem., Int. Ed.* **2003**, *42*, 428. (c) Bu, X.-H.; Chen, W.; Lu, S.-L.; Zhang, R.-H.; Liao, D.-Z.; Bu, W.-M.; Shionoya, M.; Brisse, F.; Ribas, J. *Angew. Chem., Int. Ed.* **2001**, *40*, 3201.

10.1021/ic0487575 CCC: $30.25
Published on Web 01/28/2005

predictability of the coordination geometry of the transition metals compared to the inherently flexible coordination geometry of lanthanide ions.[4] However, the flexibility of the lanthanide ions combined with the rigidity of the transition metal ions can be profitable in giving a variety of structures dictated by the different size of the lanthanide ions and can result in fascinating and interesting structures. Furthermore, specific properties of lanthanide polymeric complexes resulting from this kind of coordination chemistry promise to be rich and versatile, and hence studies in this respect are increasing rapidly.[4−6] The different coordination modes of lanthanide ions with carboxylate-based ligands, especially benzenepolycarboxylates,[7] have been widely employed to construct lanthanide coordination polymers over the past decade. More recently, a fascinating assortment of novel lanthanide coordination network structures has been achieved by the use of pyridine *N*-oxide-based ligands.[8] Following the variety of compound obtained by pyridinecarboxylates and lately by the pyridine *N*-oxide, we were inspired to widen our interest by choosing isonicotinate *N*-oxide (INO), which combines both carboxylate and *N*-oxide binding units, to construct lanthanide coordination polymers. Our original aim was to combine lanthanide ions and manganese(II) to study (a) if there is any specificity in the coordination of the carboxylate versus the *N*-oxide for the metals, (b) to synthesize Mn−Ln heterometallic coordination polymers, (c) to create a novel molecular magnet (ferrimagnet) based on the different moment carriers of the two types of metals, and (d) to introduce a ligand with a large electric dipole in the search for possible nonlinear optical activity in the coordination polymers. However, we were surprised to find that the manganese ion was not present in all the compounds prepared. Consequently, we replaced the manganese sulfate with sodium sulfate to show that the same compounds were obtained.

Anion binding and the structure-determining role of anions are not new and have attracted some attention.[9] A considerable range of anions is known to act as bridges in inorganic lattices and organic−inorganic compounds; well-known and constantly used inorganic ligands are phosphates,[10] halides,[11] and sulfate,[12] while for organic ligands there are cyanide, polycyanide (dca, tcm, etc.),[13] azide,[14] oxalate,[15] and so on. It is evident that anions, incorporated as inorganic components, do not act simply as a passive constituent but rather contribute to the increased complexity and hence functionality and exert a synergistic influence at the structure-determining organic−inorganic interface. The sulfate ion, as a simple tetrahedral oxoanion, has been found to serve as auxiliary bridges in construction of transition-metal hydroxysulfates[16] and some 2D- or 3D-coordination networks with *N*, *N*′-bidentate spacers.[17] It can coordinate in a number of ways, such as monodentate, bidentate bridging, bidentate chelating, and tridentate bridging, etc., contributing to the intricacy of the final networks. It is known to bridge up to six metal ions.[18] Considering the high oxyphilic coordination behavior of lanthanide ions, it is expected that the versatile behavior of sulfate ion in conjunction with the flexibility coordination of lanthanide ions may lead to a diversity of structure frameworks, such as 3D or layered structures, as

(3) (a) Wells, A. F. In *Three-Dimensional Nets and Polyhedra*; Wiley-Interscience: New York, 1977. (b) Wells, A. F. *Further Studies of Three-dimensional Nets*; American Crystallographic Association: Pittsburgh, PA (distributed by Polycrystal Book Service), 1979. (c) Batten, S. R.; Robson, R. *Angew. Chem., Int. Ed.* **1998**, *11*, 1460.

(4) For examples, see: (a) Piguet, C.; Bünzli, J.-C. G.; Bernardinelli, G.; Hopfgartner, G.; Petoud, S.; Schaad, O. *J. Am. Chem. Soc.* **1996**, *118*, 6681. (b) Piguet, C.; Minten, E. R.; Bernardinelli, G.; Bünzli, J.-C. G.; Hopfgartner, G. *J. Chem. Soc., Dalton Trans.* **1997**, 421. (c) Renaud, F.; Piguet, C.; Bernardinelli, G.; Bünzli, J.-C. G.; Hopfgartner, G. *J. Am. Chem. Soc.* **1999**, *121*, 9326.

(5) (a) He, Z.; He, C.; Gao, E.-Q.; Wang, Z.-M.; Yang, X.-F.; Liao, C.-S.; Yan, C.-H. *Inorg. Chem.* **2003**, *42*, 2206. (b) Gheorghe, R.; Andruh, M.; Müller, A.; Schmidtmann, M. *Inorg. Chem.* **2002**, *41*, 5314. (c) Goodgame, D. M. L.; Grachvogel, D. A.; White, A. J. P.; Williams, D. J. *Inorg. Chem.* **2001**, *40*, 6180. (d) Liang, Y. C.; Cao, R.; Su, W. P.; Hong, M. C.; Zhang, W. J. *Angew. Chem., Int. Ed.* **2000**, *39*, 3304.

(6) (a) Orr, G. W.; Barbour, L. J.; Atwood, J. L. *Science* **1999**, *285*, 1049. (b) Ma, B.-Q.; Shun, D.-S.; Gao, S.; Jin, T.-Z.; Yan, C.-H.; Xu, G.-X. *Angew. Chem., Int. Ed.* **2000**, *39*, 3644.

(7) For examples, see: (a) Reineke, T. M.; Eddaoudi, M.; Moler, D.; O′Keeffe, M.; Yaghi, O. M. *J. Am. Chem. Soc.* **2000**, *122*, 4843. (b) Sun, D.-F.; Cao, R.; Liang, Y.-C.; Shi, Q.; Hong, M.-C. *J. Chem. Soc., Dalton Trans.* **2002**, 1847. (c) Wan, Y.-H.; Zhang, L.-P.; Jin, L.-P.; Gao, S.; Lu, S.-Z. *Inorg. Chem.* **2003**, *42*, 4985.

(8) (a) Long, D.-L.; Blake, A. J.; Champness, N. R.; Wilson, C.; Schröder, M. *Angew. Chem., Int. Ed.* **2001**, *40*, 2443. (b) Long, D.-L.; Blake, A. J.; Champness, N. R.; Schröder, M. *J. Am. Chem. Soc.* **2001**, *123*, 3401. (c) Long, D.-L.; Hill, R. J.; Blake, A. J.; Champness, N. R.; Hubberstey, P.; Proserpio, D. M.; Wilson, C.; Schröder, M. *Angew. Chem., Int. Ed.* **2004**, *43*, 1851.

(9) Viler, R.; Mingos, D. M. P.; White, A. J. P.; Williams, D. J. *Angew. Chem., Int. Ed.* **1998**, *37*, 1258 and refs. therein.

(10) (a) Cheetham, A. K.; Ferey, G.; Loiseau, T. *Angew. Chem., Int. Ed.* **1999**, *38*, 3268. (b) Rao, C. N. R.; Natarajan, S.; Choudhury, A.; Neeraj, S.; Ayi, A. A. *Acc. Chem. Res.* **2001**, *34*, 80.

(11) (a) Kagan, C. R.; Mitzi, D. B.; Dimitrakopoulos, C. D. *Science* **1999**, *286*, 945. (b) Xu, Z.-T.; Mitzi, D. B. *Inorg. Chem.* **2003**, *42*, 6589. (c) Xu, Z.-T.; Mitzi, D. B. *Chem. Mater.* **2003,** *15*, 3632.

(12) (a) Paul, G.; Choudhury, A.; Sampathkumaran, E. V.; Rao, C. N. R. *Angew. Chem., Int End.* **2002**, *41*, 4297. (b) Paul, G.; Choudhury, A.; Rao, C. N. R. *J. Chem. Soc., Dalton Trans.* **2002**, 3859. (c) Paul, G.; Choudhury, A.; Rao, C. N. R. *Chem. Mater.* **2003**, *15*, 1174. (d) Behera, J. N.; Paul, G.; Choudhury, A.; Rao, C. N. R. *Chem. Commun.* **2004**, 456.

(13) For recent reviews, see (a) Ohba, M.; Ōkawa, H. *Coord. Chem, Rev.* **2000**, *198*, 313. (b) Miller, J. S.; Manson, J. L. *Acc. Chem. Res.* **2001**, *34*, 563. (c) Batten, S. R.; Murray, K. S. *Coord. Chem. Rev.* **2003**, *246*, 103. (d) Sato, O. *Acc. Chem. Res.* **2003**, *36*, 692.

(14) (a) Ribas, J.; Escuer, A.; Monfort, M.; Vicente, R.; Cortés, R.; Lezama, L.; Rojo, T. *Coord. Chem. Rev.* **1999**, *193*−*195*, 1027. (b) Hong, C. S.; Do, Y. *Angew. Chem., Int. Ed*. **1999**, *38*, 193. (c) Han, S.; Manson, J. L.; Kim, J.; Miller, J. S. *Inorg. Chem.* **2000**, *39*, 4182. (d) Gao, E.-Q.; Yue, Y.-F.; Bai, S.-Q.; He, Z.; Yan, C.-H. *J. Am. Chem. Soc.* **2004**, *126*, 1419.

(15) (a) Rao, C. N. R.; Natarajan, S.; Vaidhyanathan, R. *Angew. Chem., Int. Ed*. **2004**, *43*, 1466. (b) Tamaki, H.; Zhong, Z. H.; Matsumoto, N.; Kida, S.; Koikawa, K.; Achiwa, N.; Okawa, H. *J. Am. Chem. Soc*. **1992**, *114*, 6974. (c) Mathoniere, C.; Nuttall, C. J.; Carling, S. G.; Day, P. *Inorg. Chem*. **1996**, *35*, 1201. (d) Decurtins, S.; Schmalle, H. W.; Schneuwly, O.; Ensling, J.; Gutlich, P. *J. Am. Chem. Soc.* **1994**, *116*, 9521.

(16) (a) Grohol, D.; Papoutsakis, D.; Nocera, D. G. *Angew. Chem., Int. Ed.* **2001**, *40*, 1519. (b) Frunzke, J.; Hansen, T.; Harrison, A.; Lord, J. S.; Oakley, G. S.; Visser, D.; Wills, A. S. *J. Mater. Chem.* **2001**, *11*, 179. (c) Louër, D.; Rius, J.; Bénard-Rocherullé, P.; Louër, M. *Powder Diffr*. **2001**, *16*, 86 and references therein. (d) Vilminot, S.; Richard-Plouet, M.; André, G.; Swierczynski, D.; Guillot, M.; Bourée-Vigneron, F.; Drillon, M. *J. Solid State Chem.* **2003**, *170*, 255.

(17) (a) Hagrman, D.; Hammond, R. P.; Haushalter, R.; Zubieta, J. *Chem. Mater*. **1998**, *10*, 2091. (b) Huang, S.-P. D.; Xiong, R.-G.; Sotero, P. H. *J. Solid State Chem.* **1998**, *138*, 361. (c) Laskoski, M. C.; LaDuca, R. L., Jr.; Rarig, R. S., Jr.; Zubieta, J. *J. Chem. Soc., Dalton Trans*. **1999**, 3467. (d) Tong, M.-L.; Chen, X.-M. *CrystEngComm* **2000**, 1.

(18) (a) Salah, M. B.; Vilminot, S.; Mhiri, T.; Kurmoo, M. *Eur. J. Inorg. Chem*. **2004**, 2272. (b) Zhang, Q.-Z.; Lu, C.-Z.; Yang, W.-B.; Chen, S.-M.; Yu, Y.-Q. *Inorg. Chem. Commun.* **2004**, *7*, 889.

exemplified by some amine-templated lanthanum sulfates reported by Rao and Louër et al.[19]

In this paper, we report the hydrothermal syntheses, structures, and properties of a series of three-dimensional lanthanide coordination polymers with the general formula $[Ln(INO)(H_2O)(SO_4)]_n$, incorporating both organic INO^- and inorganic sulfate bridging tectons. The compounds are labeled **1**·La, **2**·Ce, **3**·Pr, **4**·Nd, **5**·Sm, **6**·Eu, **7**·Gd, **8**·Tb, **9**·Dy, **10**·Ho, **11**·Er, **12**·Tm, **13**·Yb, and **14**·Lu for the members in the series, and all lanthanide ions are trivalent. These compounds represent good examples of the effect of the lanthanide contraction;[20] i.e., the contraction of the lanthanide ions in radius imposes evident influences upon the coordination geometry and the global network structures. In general, the lanthanide series can be divided into three groups according to their masses: the light La−Pm, the intermediate Sm−Dy, and the heavy Ho−Lu. Indeed, the title compounds can be grouped into three types: the large La, Ce, and Pr lanthanides form type I; the intermediate ones, Nd, Sm, Eu, Gd, and Tb, form type II; and the small ones, Dy, Ho, Er, Tm, Yb, and Lu, form type III. In addition, INO ligand and sulfate ion show exceptional abilities as versatile bridges to link two or more metallic centers in different modes, which contribute to the complexity and diversity of the coordination frameworks.

Experimental Section

Materials and Apparatus. $LnCl_3·6H_2O$ (Ln = Pr, Nd, Sm, Eu, Gd, Dy, Ho, Er, Tm, Yb, and Lu) were prepared by dissolving lanthanide oxide in dilute hydrochloric acid and drying. $Tb(ClO_4)_3·6H_2O$ were prepared by dissolving lanthanide oxide in dilute perchloride acid and drying. **Caution!** The perchlorate is potentially explosive. They should be prepared in small quantities and handled with care. $LaCl_3·6H_2O$, $Ce(NO_3)_3·6H_2O$, and other chemicals for the synthesis were commercially available and used without further purification. Elemental analyses (C, H, N) were performed on an Elementar Vario EL analyzer. IR spectra were recorded on a Nicolet Magna-IR 750 spectrometer equipped with a Nic-Plan Microscope. Temperature- and field-dependent magnetic measurements of compound **4**·Nd, **6**·Eu, and **13**·Yb were carried out on an Oxford MagLab 2000 magnetometer and that of **7**·Gd on a Quantum Design MPMS-5XL SQUID system. Fluorescence spectra of **6**·Eu and **8**·Tb were recorded on a Hitachi F-4500 spectrophotometer equipped with a 150 W Xe-arc lamp at room temperature, and the pallets were sealed in a solid sample holder with a quartz window. The thermal properties were investigated by a SDT2960 thermal analyzer under flowing air at a heating rate of 10 °C/min.

Preparation. All the compounds of $[Ln(INO)(H_2O)(SO_4)]_n$ were prepared by hydrothermal reaction. Typically for $[La(INO)(H_2O)(SO_4)]_n$ (**1**·La), the mixture of $LaCl_3·6H_2O$ (0.3 mmol), $MnCO_3$ (0.1 mmol), $MnSO_4·H_2O$ (0.1 mmol), HINO (0.3 mmol), H_2O (6 mL), and ethanol (6 mL) was sealed in a Teflon-lined stainless steel vessel (23 mL), heated at 155 °C for 3 days under autogenous pressure, and then cooled to room temperature. Colorless block crystals of **1**·La were harvested in a yield of 26% based on La. Similar procedures employing other lanthanide salts produced crystals of $[Ln(INO)(H_2O)(SO_4)]_n$ in yields of 22−34%, except for the cases of **2**·Ce, **5**·Sm, and **9**·Dy compounds, where it is difficult to obtain enough amount of pure phases for elemental analysis. Anal. Calcd for **1**·La, $C_6H_6NO_8LaS$: C, 18.43; H, 1.55; N, 3.58. Found: C, 18.49; H, 1.69; N, 3.57%. IR bands (cm^{-1}) for **1**·La: 3422m, 1618vs, 1557m, 1402vs, 1233vs, 1194vs, 1152vs, 1125vs, 1025m, 986m, 866m, 789 m. IR bands (cm^{-1}) for **2**·Ce: 3409m, 1619vs, 1557w, 1403vs, 1234vs, 1194vs, 1153vs, 1135vs, 1028m, 987m, 866m, 789m. Anal. Calcd for **3**·Pr, $C_6H_6NO_8PrS$: C, 18.33, H, 1.54, N, 3.56. Found: C, 18.52, H, 1.50, N, 3.37%. IR bands (cm^{-1}) for **3**·Pr: 3405m, 1619s, 1556m, 1403s, 1233s, 1194s, 1153s, 1127s, 1028m, 988m, 866m, 788m. Anal. Calcd for **4**·Nd, $C_6H_6NO_8NdS$: C, 18.18, H, 1.53, N, 3.53. Found: C, 18.06, H, 1.32, N, 3.44%. IR bands (cm^{-1}) for **4**·Nd: 3390m, 1613m, 1597m, 1544m, 1412s, 1260m, 1174m, 1152vs, 1075m, 984m, 888w, 877 m, 786m, 666s, 655m. Anal. Calcd for **6**·Eu, $C_6H_6NO_8EuS$: C, 17.83, H, 1.50, N, 3.47. Found: C, 17.72, H, 1.48, N, 3.51%. IR bands (cm^{-1}) for **6**·Eu: 3388m, 1613m, 1599m, 1544m, 1417s, 1262s, 1151vs, 1090s, 984m, 889m, 878m, 786m, 667s, 655m. Anal. Calcd for **7**·Gd, $C_6H_6NO_8GdS$: C, 17.60, H, 1.48, N, 3.42. Found: C, 17.51, H, 1.28, N, 3.51%. IR bands (cm^{-1}) for **7**·Gd: 3391m, 1614 w, 1599m, 1543m, 1441m, 1418vs, 1263s, 1171m, 1149s, 1061m, 985m, 890w, 880m, 786m, 668m. Anal. Calcd for **8**·Tb, $C_6H_6NO_8TbS$: C, 17.53, H, 1.47, N, 3.41. Found: C, 17.51, H, 1.76, N, 3.39%. IR bands (cm^{-1}) for **8**·Tb: 3403m, 1614w, 1599m, 1543m, 1443m, 1421vs, 1264s, 1192m, 1141s, 1053m, 983w, 880w, 787w, 667m, 656m. Anal. Calcd for **10**·Ho, $C_6H_6NO_8HoS$: C, 17.28, H, 1.45, N, 3.36. Found: C, 17.27, H, 1.95, N, 3.25%. IR bands (cm^{-1}) for **10**·Ho: 3328m, 3100m, 1656m, 1626m, 1558m, 1413vs, 1220m, 1160s, 1153s, 1037m, 867w, 787w, 683w, 661w. Anal. Calcd for **11**·Er, $C_6H_6NO_8ErS$: C, 17.18, H, 1.44, N, 3.34. Found: C, 17.11; H, 1.30; N, 3.25%. IR bands (cm^{-1}) for **11**·Er: 3326m, 3113m, 1644s, 1616m, 1563m, 1417vs, 1251m, 1238m, 1183m, 1138 vs, 1092s, 873w, 785w, 683w, 659w. Anal. Calcd for **12**·Tm, $C_6H_6NO_8TmS$: C, 17.11, H, 1.44, N, 3.33. Found: C, 17.09; H, 1.57; N, 3.24%. IR bands (cm^{-1}) for **12**·Tm: 3314w, 3118w, 1640m, 1617 w, 1564w, 1420s, 1237m, 1183m, 1147vs, 1126s, 1093s, 872w, 785w, 682w. Anal. Calcd for **13**·Yb, $C_6H_6NO_8YbS$: C, 16.95, H, 1.42, N, 3.29. Found: C, 16.92; H, 1.24; N, 3.19%. IR bands (cm^{-1}) for **13**·Yb: 3474m, 3112m, 1644s, 1616 m, 1563m, 1416vs, 1249m, 1237m, 1186m, 1159s, 1126vs, 1109s, 873w, 787w, 684w. Anal. Calcd for **14**·Lu, $C_6H_6NO_8LuS$: C, 16.87, H, 1.42, N, 3.28. Found: C, 16.80; H, 1.63; N, 3.19%. IR bands (cm^{-1}) for **14**·Lu: 3321w, 3118w, 1649s, 1618w, 1566w, 1421vs, 1237m, 1183m, 1164s, 1148vs, 1095s, 873w, 787w, 683w.

X-ray Crystallography. Diffraction intensity data of the single crystals were collected at room temperature on a Nonius Kappa CCD diffractometer equipped with graphite-monochromated Mo Kα radiation (λ = 0.71073 Å). Empirical absorption corrections were applied using the Sortav program.[21] All structures were solved by the direct method and refined by the full-matrix least-squares method on F^2 with anisotropic thermal parameters for all non-hydrogen atoms.[22] Hydrogen atoms were added geometrically and

(19) (a) Govindarajan, S.; Patil, K. C.; Manohar, H.; Werner, P.-E. *J. Chem. Soc., Dalton Trans.* **1986**, 119. (b) Bénard-Rocherullé, P.; Tronel, H.; Louër, D. *Powder Diffr.* **2002**, *17*, 210. (c) Bataille, T.; Louër, D. *J. Mater. Chem.* **2002**, *12*, 3487. (d) Xing, Y.; Shi, Z.; Li, G.; Pang, W. *Dalton. Trans.* **2003**, 940. (e) Dan, M.; Behera, J. N.; Rao, C. N. R. *J. Mater. Chem.* **2004**, *14*, 1257. (f) Bataille, T.; Louër, D. *J. Solid State Chem.* **2004**, *177*, 1235.

(20) (a) Pan, L.; Huang, X.-Y.; Li, J.; Wu, Y.-G.; Zheng, N.-W. *Angew. Chem., Int. Ed.* **2000**, *39*, 527. (b) Dimos, A.; Tsaousis, D.; Michaelides, A.; Skoulika, S.; Golhen, S.; Ouahab, L.; Didierjean, C.; Aubry, A. *Chem. Mater.* **2002,** *14*, 2616. (c) Liu, Q.-D.; Gao, S.; Li, J.-R.; Ma, B.-Q.; Zhou, Q.-Z.; Yu, K.-B. *Polyhedron* **2002**, *21*, 1097. (d) Thirumurugan, A.; Natarajan, S. *Eur. J. Inorg. Chem.* **2004**, 762.

(21) (a) Blessing, R. H. *Acta Crystallogr.* **1995**, *A51*, 33. (b) Blessing, R. H. *J. Appl. Crystallogr.* **1997**, *30*, 421.

Table 1. Crystallographic Data of Complexes 1·La−14·Lu

	1·La	**2**·Ce	**3**·Pr	**4**·Nd	**5**·Sm
formula	$C_6H_6NO_8LaS$	$C_6H_6NO_8CeS$	$C_6H_6NO_8PrS$	$C_6H_6NO_8NdS$	$C_6H_6NO_8SmS$
fw	391.09	392.30	393.09	396.42	402.53
crystal system	triclinic	triclinic	triclinic	monoclinic	monoclinic
space group, *Z*	$P\bar{1}$, 2	$P\bar{1}$, 2	$P\bar{1}$, 2	$P2_1/c$, 4	$P2_1/c$, 4
a (Å)	6.6774(3)	6.6459(2)	6.6182(2)	7.7941(1)	7.7706(2)
b (Å)	7.3389(4)	7.3040(2)	7.2788(2)	20.7801(5)	20.6308(7)
c (Å)	10.4329(6)	10.3885(3)	10.3611(3)	6.3806(2)	6.3439(2)
α (deg)	77.323(2)	77.3540(10)	77.3539(13)	90	90
β (deg)	87.664(2)	87.4134(11)	87.3002(12)	106.6700(8)	106.7118(14)
γ (deg)	89.533(3)	89.8783(14)	90.0259(15)	90	90
V (Å^3)	498.38(5)	491.53(2)	486.44(2)	989.98(4)	974.06(5)
ρ_{calcd} (g cm^{-3})	2.606	2.651	2.684	2.660	2.745
μ (mm^{-1})	4.528	4.876	5.256	5.489	6.277
R1[a] [$I > 2\sigma(I)$]	0.0327	0.0272	0.0369	0.0294	0.0405
wR2[b] (all data)	0.0515	0.0630	0.0805	0.0633	0.0869
GOF	0.927	1.063	1.022	0.950	0.928

	6·Eu	**7**·Gd	**8**·Tb	**9**·Dy	**10**·Ho
formula	$C_6H_6NO_8EuS$	$C_6H_6NO_8GdS$	$C_6H_6NO_8TbS$	$C_6H_6NO_8DyS$	$C_6H_6NO_8HoS$
fw	404.14	409.43	411.10	414.68	417.11
crystal system	monoclinic	monoclinic	monoclinic	monoclinic	monoclinic
space group, *Z*	$P2_1/c$, 4	$P2_1/c$, 4	$P2_1/c$, 4	$P2_1/c$, 4	$P2_1/c$, 4
a (Å)	7.7564(2)	7.7500(1)	7.7370(3)	9.3243(2)	9.3076(2)
b (Å)	20.5503(5)	20.4884(5)	20.3121(6)	14.7539(4)	14.7214(3)
c (Å)	6.3399(3)	6.3379(2)	6.3704(2)	7.6322(4)	7.6176(2)
α (deg)	90	90	90	90	90
β (deg)	106.8235(10)	106.7190(10)	106.3832(10)	100.4356(13)	100.4505(9)
γ (deg)	90	90	90	90	90
V (Å^3)	967.31(6)	963.82(4)	960.49(6)	1032.59(6)	1026.46(4)
ρ_{calcd} (g cm^{-3})	2.775	2.822	2.843	2.667	2.699
μ (mm^{-1})	6.734	7.132	7.615	7.470	7.944
R1[a] [$I > 2\sigma(I)$]	0.0359	0.0314	0.0395	0.0284	0.0252
wR2[b] (all data)	0.0813	0.0646	0.0806	0.0518	0.0515
GOF	0.945	0.925	0.903	0.929	0.956

	11·Er	**12**·Tm	**13**·Yb	**14**·Lu
formula	$C_6H_6NO_8ErS$	$C_6H_6NO_8TmS$	$C_6H_6NO_8YbS$	$C_6H_6NO_8LuS$
fw	419.44	421.11	425.22	427.15
crystal system	monoclinic	monoclinic	monoclinic	monoclinic
space group, *Z*	$P2_1/c$, 4	$P2_1/c$, 4	$P2_1/c$, 4	$P2_1/c$, 4
a (Å)	9.2921(2)	9.2764(4)	9.2635(2)	9.2534(4)
b (Å)	14.6877(3)	14.6665(9)	14.6315(4)	14.6087(5)
c (Å)	7.6046(2)	7.5969(6)	7.5815(3)	7.5751(2)
α (deg)	90	90	90	90
β (deg)	100.4473(9)	100.370(2)	100.3649(12)	100.4133(12)
γ (deg)	90	90	90	90
V (Å^3)	1020.67(4)	1016.69(11)	1010.82(5)	1007.14(6)
ρ_{calcd} (g cm^{-3})	2.730	2.751	2.794	2.817
μ (mm^{-1})	8.459	8.964	9.491	10.042
R1[a] [$I > 2\sigma(I)$]	0.0223	0.0320	0.0338	0.0317
wR2[b] (all data)	0.0473	0.0531	0.0632	0.0556
GOF	0.994	0.866	0.872	0.913

[a] $R1 = \sum||F_o| - |F_c||/\sum|F_o|$. [b] $wR2 = \{\sum[w(F_o^2 - F_c^2)^2]/\sum[w(F_o^2)^2]\}^{1/2}$.

refined using the riding model. The details of crystallographic data and structure refinement results are summarized in Table 1.

Results and Discussion

The series compounds, [Ln(INO)(H$_2$O)(SO$_4$)]$_n$ (Ln = La−Lu except for Pm, all ions are trivalent), were surprisingly obtained by the hydrothermal reaction of Ln^{3+}, $MnCO_3$, $MnSO_4$·H$_2$O, and HINO in a mixture of water and ethanol instead of the aimed Mn−Ln heterometallic coordination polymers. This finding shows that there is a greater affinity for lanthanides to coordinate to the INO ligand than the transition metals. While replacing the manganese sulfate by sodium sulfate works in the same way, changing the solvent results in different structural types, and these will be reported shortly. Interestingly, both INO and SO_4^{2-} act as bridges with different modes of coordination (Chart 1), resulting in the flexibility of the structures. The key feature of this study is the segregation into three structural types depending solely on the size of the metal ions, demonstrating the lanthanide contraction effect. In the following we describe a representative for each structural types.

Type I Structure of 1·La, 2·Ce, and 3·Pr. The key feature of the type I structure, represented by compound

(22) (a) Sheldrick, G. M. *SHELXTL* Version 5.1. Bruker Analytical X-ray Instruments Inc., Madison, Wisconsin, USA, 1998. (b) Sheldrick, G. M. *SHELXL-97*, PC Version. University of Göttingen, Germany, 1997.

Chart 1. Coordination Modes of INO Ligand and SO_4^{2-} Anion Observed in Complexes **1**·La−**14**·Lu

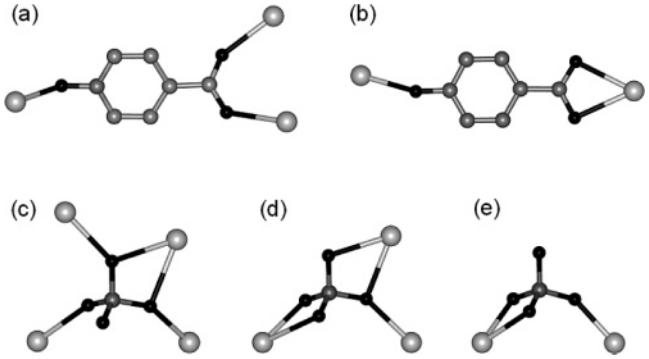

1·La, is a three-dimensional framework consisting of inorganic layers of Ln and SO_4^{2-} pillared by the organic INO. As shown in Figure 1a, each La(III) ion is nine-coordinated in a triply capped trigonal prism by one *N*-oxide oxygen atom from one INO ligand, two carboxylate oxygen atoms from two INO ligands, five oxygen atoms from four SO_4^{2-} anions, and one oxygen atom from a coordinated water molecule.

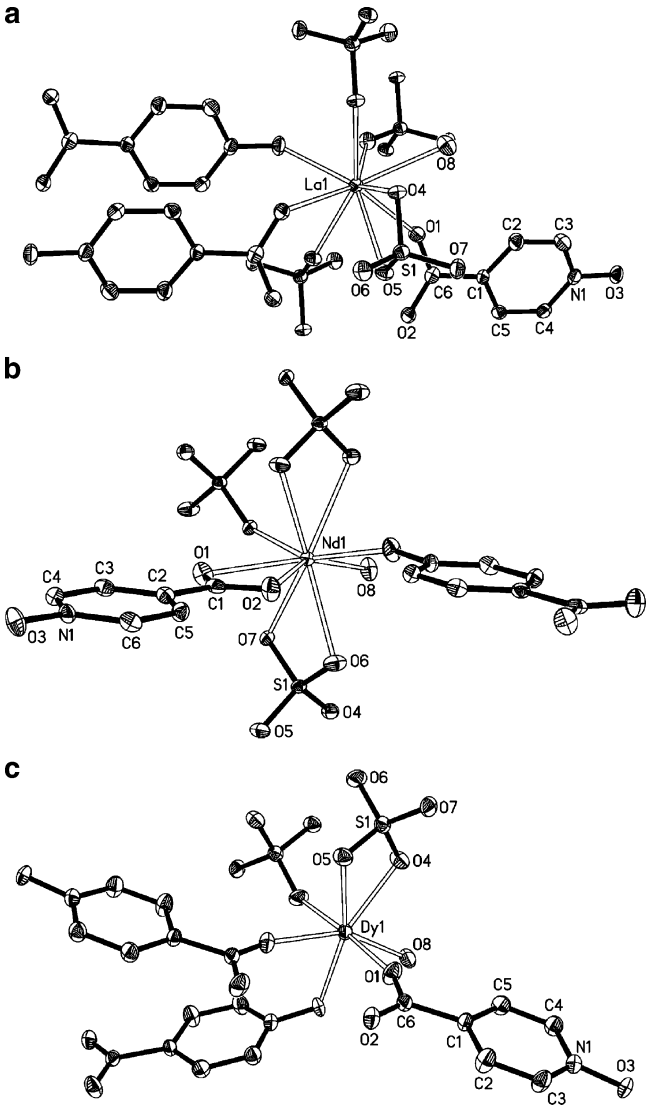

Figure 1. Local coordination environment of compounds **1**·La, **4**·Nd, and **9**·Dy with 40% thermal ellipsoids. Hydrogen atoms are omitted for clarity.

Table 2. Selected Bond Lengths for Compounds **1**·La−**3**·Pr[a]

bond		distance (Å) **1**·La	**2**·Ce	**3**·Pr
Ln(1)−O(2A)		2.543(3)	2.519(3)	2.496(4)
Ln(1)−O(5A)		2.560(3)	2.541(2)	2.525(4)
Ln(1)−O(4B)		2.587(3)	2.564(2)	2.554(4)
Ln(1)−O(6C)		2.487(3)	2.484(3)	2.467(4)
Ln(1)−O(3D)		2.472(3)	2.441(2)	2.426(4)
Ln(1)−O(1)		2.449(3)	2.423(2)	2.408(4)
Ln(1)−O(4)		2.635(3)	2.618(2)	2.602(4)
Ln(1)−O(5)		2.691(3)	2.671(2)	2.648(4)
Ln(1)−O(8)		2.617(4)	2.600(3)	2.588(4)
duadruply bridged Ln1···Ln1A		4.255(6)	4.224(3)	4.201(3)
doubly bridged Ln1···Ln1B		4.447(6)	4.417(3)	4.392(3)
interplanar Py···Py		3.27, 3.20	3.25, 3.18	3.23, 3.17
O(8)−H···O(2)#1	O···O distance	2.813	2.792	2.786
hydrogen bond	O−H···O angle	157	162	147
C(3)−H···O(7)#2	C···O distance	3.098	3.099	3.101
hydrogen bond	C−H···O angle	161	160	158
O(4)−H···O(7)#3	C···O distance	3.239	3.242	3.227
hydrogen bond	C−H···O angle	173	173	173

[a] Symmetry transformations used to generate equivalent atoms (consistent with the symmetry transformations in Figure 2): (A) $-x+1, -y+1, -z$; (B) $-x+1, -y+2, -z$; (C) $x-1, y, z$; (D) $x, y, z+1$; (#1) $x, y+1, z$; (#2) $-x+1, -y+2, -z-1$; (#3) $-x+1, -y+1, -z-1$.

Therefore, the ligands around La(III) ion are three INO, four sulfate ions, and one water. The La−O distances (Table 2) range from 2.449(3) to 2.691(3) Å (average value 2.560(3) Å), and the longer La−O distances are associated with the sulfate oxygen atoms, O4 and O5, each of which acts as a μ_2-O bridge linking two La centers. The O−La−O bond angles range from 52.43(8)° to 152.28(9)°.

The 3D framework can be considered as inorganic La−SO_4−H_2O layers pillared by organic INO ligands. The inorganic layer (Figure 2) consists of $[La(SO_4)(H_2O)]_\infty$ chains running along the *b* direction linked together in the *a* direction. Within the chain, La(III) ions are arranged zigzag-like, and each pair of La ions is bridged by two μ_2-O bridges of two SO_4^{2-} anions to form a $[La_2O_2]$ rhombic unit. These units form the chain by sharing their two apexes (La^{3+} ions) of acute angle. SO_4^{2-} anions are also in a zigzag-like arrangement complementary to the zigzag array of La ions; therefore, each SO_4^{2-} anions provides two μ_2-O atoms (O4 and O5) to bridge three La ions of a triangle in the chain. It is worth noting that half the $[La_2O_2]$ rhombic units have two additional La−O−C−O−La connectivities by two carboxyl groups of INO pillars in a syn−syn bridging mode.[23] Therefore, the doubly carboxyl-bridged $[La_2O_2]$ units and those not carboxyl-bridged arrange alternatively along the chain. The former has a La···La separation of 4.255 Å, while the latter has a slightly longer La···La separation of 4.447 Å. The linkages of adjacent chains are via the binding of the third oxygen atoms (O6) of the SO_4^{2-} anions of one chain to the La(III) ions of the neighboring ones, on both sides of the principal chain. The fourth oxygen atom of the SO_4^{2-} anion is free of coordination but involved in the formation of hydrogen bonds discussed later. Therefore, each SO_4^{2-} anion in the structure binds four La(III) ions in an η^3,μ_4-pentadentate coordination mode (Chart 1c), providing two

(23) Carrell, C. J.; Carrell, H. L.; Erlebacher, J.; Glusker, J. P. *J. Am. Chem. Soc.* **1988**, *110*, 8651.

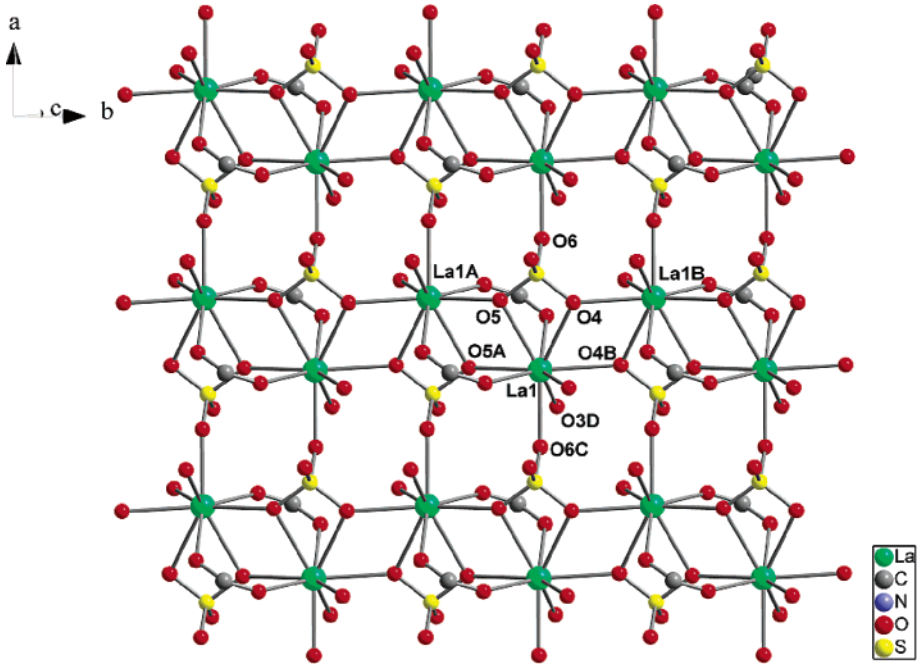

Figure 2. Two-dimensional Ln−SO$_4$−H$_2$O layer in **1**·La. Symmetry code: (A) $-x+1, -y+1, -z$; (B) $-x+1, -y+2, -z$; (C) $x-1, y, z$; (D) $x, y, z+1$.

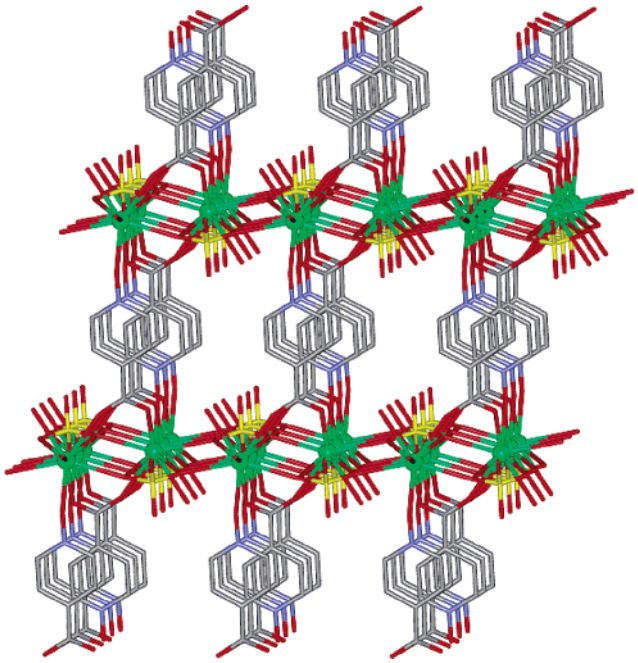

Figure 3. Three-dimensional structure of **1**·La viewed down the *a* axis. Note that the uncoordinated O atoms of SO_4^{2-} anions and bonded water molecules protrude out of the layers.

La−O−La and five additional La−O−S−O−La linkages with La···La distance of 5.672−7.339 Å. This layered structure is different from those of reported lanthanum sulfates in the literature.[19,24] The inorganic layers, parallel to the *ab* plane, are further pillared by organic INO ligands (Figure 3). The INO ligands, each having its *N*-oxide group binding one La(III) ion in one layer while its carboxylate group binding La(III) ions of the adjacent layer in a monodentate and bridging mode (Chart 1a), act as pillars linking the inorganic layers with the interlayer distance of ca. 10 Å. On the basis of such a coordination mode, an interesting three-dimensional pillared-layer framework is formed with complete segregation of organic and inorganic moieties, as found in metal−organophosphates,[25] Co−hydroxide pillared by carboxylate,[26] and layered-perovskite pillared by organoamines.[11] The INO pillars also interact with the layers via O−H···O and C−H···O hydrogen bonds, which contribute to the additional stability of the structure.[27] The O−H···O hydrogen bond involves the coordinated water oxygen O8 from the layer and the carboxylate oxygen O2 from the adjacent pillar, the O···O distance and the O−H···O angle being 2.813 Å and 157°, respectively. The C−H···O hydrogen bonds originate from the uncoordinated sulfate O7 atom and the pyridine C−H (C3 and C4) from neighboring pillars, the C3···O7 and C4···O7 distances being 3.098 and 3.239 Å and the C3−H···O7 and C4−H···O7 angles being 161 and 173°, respectively. In addition, the INO pillars are arranged in parallel in the *b* direction and in antiparallel in the *a* direction, and neighboring pyridyl rings along the *a* direction overlap with a bond-over-ring mode,[28] with the interplanar distances being alternately 3.27 and 3.20 Å, suggesting the presence of stacking $\pi-\pi$ interactions. It is worth noting that this pillared-layer structure is, to our

(24) Wickleder, M. S. *Chem. Rev.* **2002**, *102*, 2011.

(25) (a) Wang, Z.-K.; Heising, J. M.; Clearfield, A. *J. Am. Chem. Soc.* **2003**, *125*, 10375. (b) Yang, B.-P.; Mao, J.-G.; Sun, Y.-Q.; Zhao, H.-H.; Clearfield, A. *Eur. J. Inorg. Chem.* **2003**, 4211. (c) Cao, G.; Hong, H.; Mallouk, T. E. *Acc. Chem. Res.* **1992**, *25*, 420.

(26) (a) Rujiwatra, A.; Kepert, C. J.; Claridge, J. B.; Rosseinsky, M. J.; Kumagai, H.; Kurmoo, M. *J. Am. Chem. Soc.* **2001**, *123*, 10584. (b) Kumagai, H.; Oka, Y.; Inoue, K.; Kurmoo, M. *J. Chem. Soc., Dalton Trans.* **2002**, 3442. (c) Kurmoo, M.; Kumagai, H.; Hughes, S. M.; Kepert, C. J. *Inorg. Chem.* **2003**, *42*, 6709.

(27) (a) Desiraju, G. R. *Acc. Chem. Res.* **2002**, *35*, 565. (b) Steiner, T. *Angew. Chem., Int. Ed.* **2002**, *41*, 48. (c) Steiner, T. *Chem. Commun.* **1997**, 727.

(28) Janiak, C. *J. Chem. Soc., Dalton Trans.* **2000**, 3885.

Table 3. Selected Bond Lengths for Compounds **4**·Nd−**8**·Tb[a]

bond		distance (Å)				
		4·Nd	**5**·Sm	**6**·Eu	**7**·Gd	**8**·Tb
Ln(1)−O(3)#1		2.299(3)	2.272(5)	2.263(5)	2.254(4)	2.249(5)
Ln(1)−O(4)#2		2.447(3)	2.407(4)	2.390(4)	2.384(3)	2.360(5)
Ln(1)−O(6)#3		2.472(3)	2.440(4)	2.418(4)	2.396(4)	2.363(5)
Ln(1)−O(7)#3		2.712(3)	2.749(5)	2.783(5)	2.831(4)	3.044(6)
Ln(1)−O(1)		2.553(3)	2.514(5)	2.506(5)	2.491(4)	2.457(5)
Ln(1)−O(2)		2.518(3)	2.494(5)	2.481(5)	2.469(4)	2.448(5)
Ln(1)−O(4)		2.617(3)	2.599(4)	2.587(4)	2.564(3)	2.547(5)
Ln(1)−O(5)		2.538(3)	2.511(4)	2.498(4)	2.480(4)	2.448(5)
Ln(1)−O(8)		2.434(4)	2.403(6)	2.388(6)	2.367(4)	2.348(5)
binuclear Ln···Ln		4.243(1)	4.196(2)	4.166(1)	4.143(1)	4.101(1)
Ln···Ln spanned by sulfate ion		6.381(0)	6.344(1)	6.340(1)	6.338(0)	6.370(1)
Ln···Ln spanned by INO ligand		10.607(2)	10.544(3)	10.506(2)	10.483(2)	10.422(2)
interplanar Py···Py		3.18	3.16	3.16	3.16	3.20
O(8)−H···O(7)	O···O distance	2.783	2.767	2.755	2.769	2.732
hydrogen bond	O−H···O angle	178	175	158	170	175

[a] Symmetry transformations used to generate equivalent atoms: (#1) $x + 1, -y + {}^1/_2, z + {}^1/_2$; (#2) $-x, -y + 1, -z + 1$; (#3) $x, y, z + 1$.

knowledge, the first example that the organic moieties link the inorganic lanthanide sulfate layer via coordination bonds, compared to many reported layered structures of amine-template lanthanide sulfates, which are built up from anionic layers of lanthanide sulfate stabilized with organic entities in the interlayer space via hydrogen bonds.[19] Moreover, the pillaring of inorganic layers represents an important strategy for generation of porous coordination materials that may display excellent host−guest properties.[29] By modifying the anionic organic pillars with a variety of lengths and functionalities, a diversity of organically pillared lanthanide sulfate layer framework with different channel dimensions and surface properties can be expected.

Compound **2**·Ce and **3**·Pr are of the same structure as **1**·La. The selected bond lengths, together with some nonbonding separations, listed in Table 2, indicate that all the Ln−O bond lengths, the Ln···Ln separations, and the $\pi-\pi$ interacting distances between pyridine rings decrease from **1**·La to **3**·Pr, consistent with the radius contraction from La to Pr.

Type II Structure of 4·Nd, 5·Sm, 6·Eu, 7·Gd, and 8·Tb. The structure of type II, represented by compound **4**·Nd, can be described as a 2-fold interpenetrated "3D herringbone" network. As shown in Figure 1b, the coordination polyhedron around each Nd(III) ion is a triply capped trigonal prism with three sites occupied by the oxygen atom of the *N*-oxide group of an INO ligand and the chelating carboxylate group from another INO ligand and five sites by oxygen atoms from three SO_4^{2-} anions. The last site is occupied by a water molecule. Although the Nd(III) ion is still nine-coordinated, the ligands surrounding each Nd(III) are reduced to two INO, three sulfate ions, and one water, compared to those in the type I structure. The distances of Nd−O (Table 3) range from 2.299(3) to 2.712(3) Å (average value 2.510(3) Å). The longest Nd−O distance is associated with one (O7) of the sulfate oxygen atoms.

Different from the inorganic La−SO_4−H_2O layers of **1**·La, the inorganic parts of the structure of **4**·Nd are Nd−SO_4−H_2O chains along the *c* axis (Figure 4). In the chain, the $[Nd_2O_2]$ rhombic unit similar to the $[La_2O_2]$ one aforementioned are observed. The SO_4^{2-} anion not only provides one μ_2-O to form the $[Nd_2O_2]$ rhombic unit but also connects the units through its two pairs of oxygen atom to chelate the two Nd ions of adjacent $[Nd_2O_2]$ units. Therefore, the chain is ladder-like, with the $[Nd_2O_2]$ units as the rungs and Nd−O−S−O−Nd linkages as the side rails. The Nd···Nd separations are 4.243 Å in the $[Nd_2O_2]$ unit and 6.381 Å between the units, respectively. The SO_4^{2-} anion adopts an $\eta,^4\mu_3$-pentadentate coordination mode (Chart 1d), binding three Nd ions.

The 3D structure is generated by the connections of the chains via the INO ligands (Figure 5). Each INO ligand is connected with two Nd(III) ions from different chains in the monodentate (the *N*-oxide group) and chelating (the carboxyl group) mode (Chart 1b), and each Nd(III) is connected with two INO ligands. Thus, the $[Nd_2O_2]$ unit is connected to four others through four bridging INO ligands that radiate from the unit in different directions; hence, each chain is linked to four identical and parallel ones to generate a 3D structure. The $[Nd_2O_2]$ units and the INO ligands are oriented in such a way that they constitute a 2D herringbone layer parallel to the (−102) plane, with each metal ion as the node. Therefore, considering the connection via sulfate ions in the *c* direction, the global network may alternatively be described as a "3D herringbone" topology, built of 2D herringbone layers with sulfate ions as interlayer pillars. In other words, if the $[Nd_2O_2]$ unit is taken as a node and the two linkages via SO_4^{2-} between the units are considered as one connectivity, the framework can be related to α-Po type.[3]

The individual 3D network is "open" with large rectangular channels of size ca. 14.6 × 10.6 Å (based on Nd···Nd separations) along the *c* direction, and on the sidewall of the channel there also exist rectangular interchannel windows of size ca. 10.6 × 6.4 Å, ringed by four Nd(III) ions, two sulfate ions, and two INO ligands. These "empty" spaces are filled through the interpenetration of two identical nets related by the *c* slide operation (Figure 6). The ladder chains of one net thread through the channels of the other net, and the INO ligands of one net thread through the interchannel

(29) Kitagawa, S.; Kitaura, R.; Noro, S.-I. *Angew. Chem., Int. Ed.* **2004**, *43*, 2334 and refs. therein.

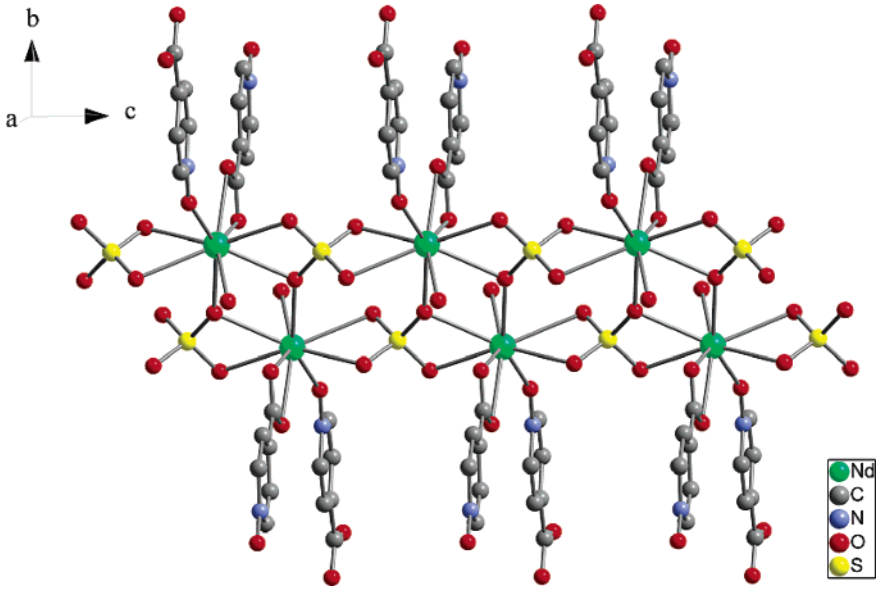

Figure 4. One-dimensional ladder-like chain in **4**·Nd, running along the *c* direction.

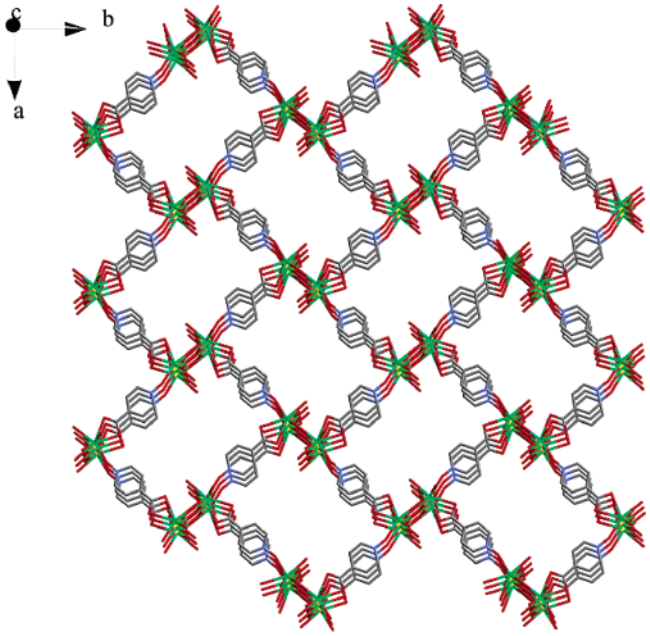

Figure 5. Individual three-dimensional framework of **4**·Nd showing the rectangular channels.

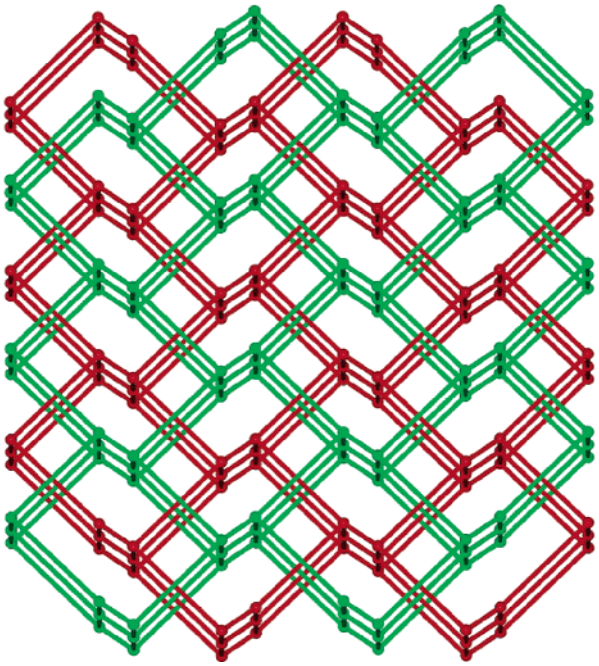

Figure 6. Topological view of the 2-fold interpenetration of the "3D herringbone" in **4**·Nd. Nodes are each metal ions and short bonds are connectivities via sulfate, while long bonds are via INO ligand.

windows of the other net. The interpenetrated structure is stabilized by extensive $\pi-\pi$ interactions and strong O−H···O hydrogen bonds. Each pyridyl ring of one net is inserted between two others from the other net in a face-to-face and partially overlapping fashion,[28] leading to one-dimensional columns of pyridyl rings stacked along the *c* direction, with an interplanar distances of 3.18 and 3.20 Å. The O−H···O hydrogen bonds originate from the coordinated water oxygen O8 from one net with O7 of the bridging SO_4^{2-} anions from the other, the O···O distance and the O−H···O angle being 2.783 Å and 178°, respectively.

Compound **5**·Sm, **6**·Eu, **7**·Gd, and **8**·Tb are isomorphous with **4**·Nd, and selected distances are listed in Table 3. As the ionic radii decreasing from Nd to Tb, all Ln−O bond lengths except for Ln−O7#3 decrease due to the lanthanide contraction, as do the Ln···Ln nonbonding separations spanned by the double μ_2-O bridge and the INO spacer. The Ln−O7#3 distance, which is the longest one among the Ln−O bonds for each compound, increases rather than decreases with increasing atomic numbers. This observation represents the result of the lanthanide contraction operating in the opposite way. Generally, the decrease in metal radius leads to the decrease in Ln−O distances. But on the other hand, this will lead to more steric hindrance due to the interligand repulsion.[20b] It is likely that the nine-coordinative environment in structure type II is somewhat crowded. As the size of the metal center decreases, one of the donor atoms tends to be squeezed outward to reduce the steric hindrance, justifying the increase of the Ln−O7#3 distance from Nd to

Table 4. Selected Bond Lengths for Compounds **9**·Dy−**14**·Lu[a]

bond		distance (Å)					
		9·Dy	**10**·Ho	**11**·Er	**12**·Tm	**13**·Yb	**14**·Lu
Ln(1)−O(6)#1		2.272(3)	2.257(3)	2.244(3)	2.230(4)	2.228(4)	2.207(4)
Ln(1)−O(2)#2		2.267(3)	2.257(3)	2.249(3)	2.228(4)	2.222(4)	2.213(4)
Ln(1)−O(3)#3		2.294(3)	2.282(3)	2.276(2)	2.269(4)	2.256(4)	2.248(4)
Ln(1)−O(1)		2.242(3)	2.232(3)	2.219(3)	2.207(4)	2.200(5)	2.187(4)
Ln(1)−O(4)		2.378(3)	2.370(3)	2.362(3)	2.344(4)	2.336(4)	2.334(4)
Ln(1)−O(5)		2.382(3)	2.368(3)	2.362(3)	2.356(4)	2.346(4)	2.338(4)
Ln(1)−O(8)		2.325(4)	2.307(3)	2.292(3)	2.290(4)	2.285(4)	2.263(4)
intradimer Ln···Ln		5.135(2)	5.125(2)	5.116(1)	5.104(3)	5.096(2)	5.091(2)
interdimer Ln···Ln		5.335(3)	5.321(2)	5.308(2)	5.300(4)	5.288(2)	5.277(2)
C(4)−H···O(5)#4	C···O distance	3.311	3.304	3.299	3.316	3.298	3.301
hydrogen bond	C−H···O angle	147	147	147	147	146	148
C(5)−H···O(7)#4	C···O distance	3.269	3.263	3.250	3.258	3.251	3.251
hydrogen bond	C−H···O angle	149	149	149	149	149	149
O(8)−H···O(7)#4	O···O distance	2.771	2.778	2.790	2.789	2.777	2.782
hydrogen bond	O−H···O angle	170	175	166	173	173	166
O(8)−H···O(7)#5	O···O distance	2.719	2.723	2.715	2.717	2.713	2.728
hydrogen bond	O−H···O angle	158	155	168	157	173	167

[a] Symmetry transformations used to generate equivalent atoms: (#1) $-x+1, -y, -z$; (#2) $-x, -y, -z$; (#3) $-x, y-{}^1/_2, -z+{}^1/_2$; (#4) $x, -y+{}^1/_2, z+{}^1/_2$; (#5) $x, y, z+1$.

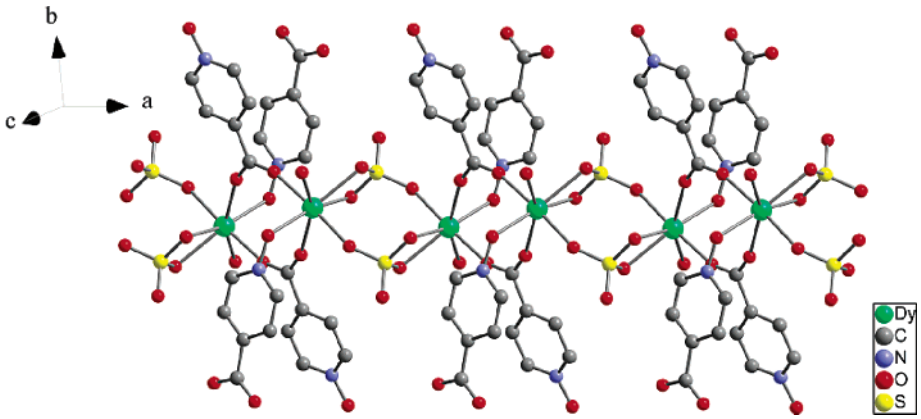

Figure 7. One-dimensional chain extending along the *a* axis in **9**·Dy.

Tb. This effect is especially obvious for the Tb complexes, in which the metal ion is the smallest for this structure type and the Ln−O7#3 distance (3.044 Å) is significantly longer than that in **4**·Nd, **5**·Sm, **6**·Eu, and **7**·Gd. The coordination number of Tb can be regarded as eight if O7#3 is not considered to be involved in the coordination environment of the Tb ion. Hence, in this type of structure, the metal coordination number changes from nine to eight, as the result of the lanthanide contraction. The irregular variation from Nd to Tb of the Ln···Ln separations spanned by sulfate ions can be attributed to the concurrence of the increase of the Ln−O7 distance and the decreases of other Ln−O distances.

Type III Structure of 9·Dy, 10·Ho, 11·Er, 12·Tm, 13·Yb, and 14·Lu. The structure of type III, represented by compound **9**·Dy, is different from those of types I and II. First of all, the local coordination environment around the Ln(III) ion is significantly different. As indicated in Figure 1c, each Dy(III) ion exhibits a pentagonal bipyrimidal coordination environment coordinated by three oxygen atoms of one *N*-oxide and two carboxyl groups from three INO ligands, three oxygen atoms from two SO_4^{2-} anions, and one oxygen atom from a coordinated water molecule. Thus, each metal center is surrounded by three INO ligands, two sulfate anions, and one water, in contrast to those in **1**·La and **4**·Nd. The distances of Dy−O (Table 4) range from 2.242(3) to 2.382(3) Å (average 2.308 Å).

Compared with the extended inorganic moieties, either a 2D layer in the type I structure or a 1D chain in the type II structure, the inorganic moiety in **9**·Dy is a discrete dimer (Figure 7), in which two Dy ions, with a separation of 5.135 Å, are bridged by a pair of SO_4^{2-} anions in a chelating-monodentate mode (Chart 1e). The dimers are further linked by two INO ligands with their carboxyl groups binding two Dy ions in a bidentate syn−syn mode to produce an infinite chain running along the *a* direction, the interdimer Dy···Dy separation being 5.335 Å. To each Dy ion another INO ligand coordinates via monodentate *N*-oxide groups, occupying the trans sites across the dimer. And it forms two C−H···O hydrogen bonds with the neighboring sulfate: one is C4−H···O5, with the C···O distance and the C−H···O angle being 3.310 Å and 147°, and the other is C5−H···O7, with the C···O distance and the C−H···O angle being 3.268 Å and 149°.

With the bridging ability of the INO ligand, each chain is connected with the four adjacent ones related to the previous one by 2_1 screw axes through INO ligands, resulting in a

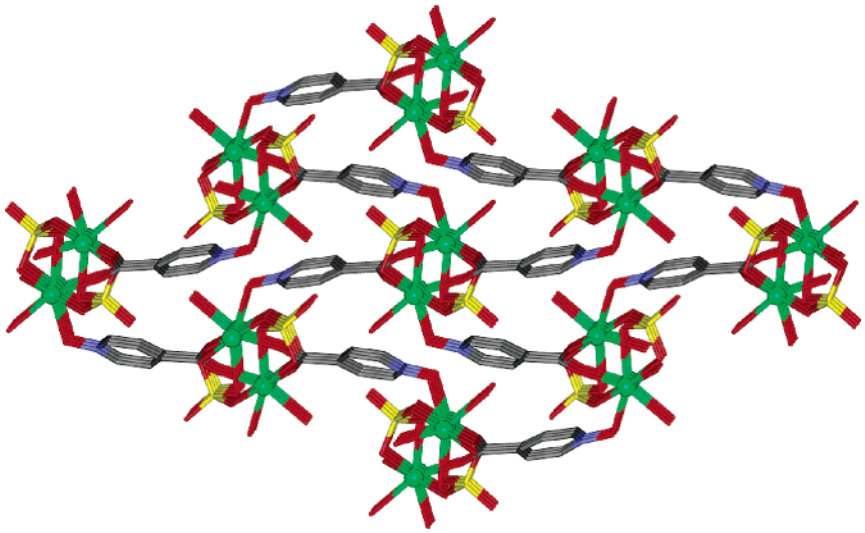

Figure 8. Three-dimensional network in **9**·Dy.

three-dimensional network (Figure 8). If the two Dy(III) ions briged by syn−syn carboxyl groups are considered to be a dinuclear unit, the network, though very distorted, can be related to α-Po when each dinuclear unit is treated as a six-connected node that is linked to four identical nodes by the INO ligands and to two others by two pairs of SO_4^{2-} anions. There exist two kinds of strong interchain hydrogen bonds that reinforce the 3D structure, both involving the coordinated water oxygen O8 and the noncoordinated sulfate oxygen O7 (Table 4). The first (O8−H···O7#4; symmetry code, x, $-y + {}^1/_2$, $z + {}^1/_2$) is between the chains linked by the INO ligands, with the O···O distance and the O−H···O angle being 2.778 Å and 175°, respectively. The other (O8−H···O7#5; symmetry code, x, y, $z + 1$) is formed between the chains related to each other by unit translation along the c direction, the O···O distance and the O−H···O angle being 2.723 Å and 155°, respectively.

Compounds **10**·Ho, **11**·Er, **12**·Tm, **13**·Yb, and **14**·Lu are isomorphous with **9**·Dy. This subseries of compounds of type III structure also show the effect of lanthanide contraction: Ln−O bond lengths and Ln···Ln separations decrease along with the decrease of ionic radii from Dy to Lu (Table 4).

Discussion on Structure Evolution. The present study consists of a complete family of 3D lanthanide compounds with the same general formula [Ln(INO)(H$_2$O)(SO$_4$)]$_n$ (Ln = La−Lu except for the radioactive and rare Pm) and demonstrate a clear effect of lanthanide contraction resulting in three structural polymorphs. All the structures consist of inorganic Ln−SO_4^{2-} skeletons connected by the organic moiety INO. The large La, Ce, and Pr lanthanides form type I structure (pillared layers); the intermediate ones, Nd, Sm, Eu, Gd, and Tb, form type II structure (doubly interpenetrated frameworks, with individual framework consisting of INO connected inorganic chains); and the small ones, Dy, Ho, Er, Tm, Yb, and Lu, form type III structure (INO connected inorganic dimers). As the ionic radii of the lanthanide ions decreases with increasing atomic number from La to Lu, the increasingly important ligand−ligand repulsion leads to the different metal coordination environments: the metal coordination number decreases from nine (types I and Nd, Sm, Eu, and Gd of type II) to eight (Tb of type II) to seven (type III), and the number of ligands around each metal ion decreases from eight (three INO ions, four sulfate ions and a water molecule for type I) to six (two INO ions, three sulfate ions, and a water molecule for type II; three INO ions, two sulfate ions and a water molecule for type III). As already mentioned, the contraction of the metal radius is also reflected in each structural type by the decrease of the bonding Ln−O and some nonbonding distances with the increasing atomic number. In fact, the general trend for Ln−O distances holds true throughout all the compounds. The exception observed in type II for the Ln−O distance has also been attributed to the lanthanide contraction. Another important aspect of the structure evolution is that the inorganic moieties of Ln−SO_4−H_2O of these structures change from 2D sheet of type I to 1D chain of type II to discrete dimer of type III.

The differences in coordination number of the lanthanide ions due to lanthanide contraction have great influences on the final structures, which are facilitated by the coordination versatility of the INO and sulfate ligands rendering them adaptable to the change of coordination geometry of lanthanide ions. As a simple tetrahedral oxoanion, the sulfate ion has been found to be a versatile building block and to exhibit diverse coordination modes.[16−18] It displays more complex coordination modes when coordinated to oxophilic lanthanide ions, as demonstrated by the present work and others,[19,24] which plays an important role in the formation of the skeleton of the resulting frameworks. The INO ligand also exhibits coordination flexibility: the carboxylate group can be chelating or bridging, and the N−O group is monodentate with variable M−O orientation. Their variable coordination modes and connectivity are directly related to the dimensionality, the topology, and the interpenetration of the resultant frameworks. In structures of type I, each sulfate ion connects four lanthanide ions through one μ_1-O and two μ_2-O atoms with one chelating and three monodentate sites, and each lanthanide ion is connected to as many as eight

others through sulfate ions, forming a 2D lanthanide−sulfate layer. On the other hand, each INO ligand acts as a μ_3-bridge with each oxygen atom as a monodentate site, and each lanthanide ion is connected to five others through three such INO ligands to generate also a 2D layer. The two layers intersect each other at the lanthanide ions to produce the 3D structure. In type III, the INO ligand adopts a similar coordination mode to give 2D Ln−INO layers similar to those in type I. In contrast, the sulfate ion connects only two lanthanide ions through three μ_1-O atoms, and each lanthanide ion is connected to only another one through a pair of sulfate ions. So no extended lanthanide−sulfate motifs are formed, and the sulfate ions serve as short pillars that join the Ln−INO layers into the 3D structure. Both the sulfate and INO ligand in type II adopt coordination modes different from those in types I and III. The sulfate ion binds three lanthanide ions through all of its oxygens (three μ_1-O and one μ_2-O atoms) with two chelating and one monodentate sites, and each lanthanide ion is connected to four others through three sulfate ions, forming 1D ladder-like lanthanide−sulfate chains. And the INO ligands act as μ_2-bridges with the carboxylate groups as chelating sites and the N−O oxygens as monodentate sites, joining the lanthanide ions into 1D zigzag Ln−INO chains and interlinking the lanthanide−sulfate ladders into a 3D network. The coordination modes of the INO and sulfate ligands are important for the occurrence of interpenetration. The high connectivity of the sulfate ion in type I leads to the formation of the dense Ln−SO_4 layers, and thus interpenetration is prevented. For type III, the absence of interpenetration may be mainly due to the relatively high connectivity in the Ln−INO linkage: the μ_3 bridging mode of the INO ligand reduces the space between neighboring metal centers, and the presence of three INO ligands around each metal ion also reduces the space between neighboring ligands. On the other hand, in type II structure, the μ_2 chelating-monodentate coordination mode of the INO ligand and the presence of only two INO ligands around each metal ion make the building units well separated in space, and in addition, the η^4,μ_3 coordination mode of the sulfate ion leads to a unique ladder, in which the two metal ions chelated on the opposite sides of the sulfate ions are also well-separated. These result in large channels or cavities that are filled through interpenetration. Finally, the presence of $\pi-\pi$ stacking interactions between pyridyl rings and/or O−H···O hydrogen bonds between the coordination water molecules and sulfate ions should have contributed to the formation of the present 3D structures, interpenetrated or not.

Thermal, IR, and Luminescent Properties. To investigate the thermal stability of these compounds, TGA−DTA experiments were performed for these materials under flowing air. Since compounds of the same structure type show similar thermal behavior, the results of three representative compounds, **1**·La of type I, **6**·Eu of type II, and **12**·Tm of type III, are discussed. The materials are thermally stable up to 200 °C for **1**·La and **12**·Tm and 300 °C for **6**·Eu and then undergo several steps of weight loss (Figure 9). The first weight loss, being an endothermic process,

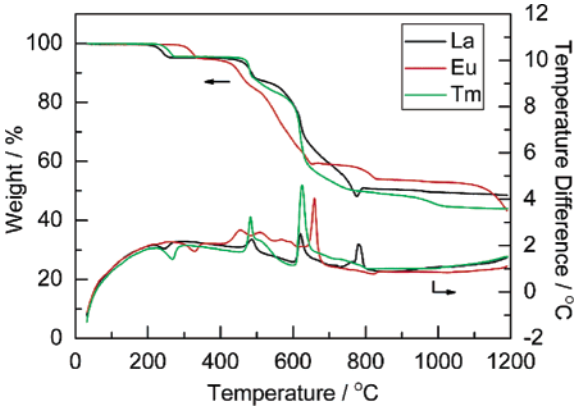

Figure 9. TGA−DTA runs of **1**·La, **6**·Eu, and **12**·Tm under air (10 °C min^{-1}).

occurred at ca. 240 °C for **1**·La and **12**·Tm, while at ca. 320 °C for **6**·Eu, corresponding to the loss of one coordinated water molecules per formula. At this step, the experimental percentage weight loss (and calculated values in parentheses) are 4.4 (4.6), 4.8 (4.5), and 4.4 (4.3) for **1**·La, **6**·Eu, and **12**·Tm, respectively. The higher stability and temperature for the release of the coordinated water molecules for **6**·Eu is due to the greater number and stronger hydrogen bonds the water molecule is involved in for **6**·Eu compared to those for **1**·La and **12**·Tm. The anhydrous phases are stable between 260 and 400 °C for **1**·La, 340 and 380 °C for **6**·Eu, and 270 and 440 °C for **12**·Tm. The followed steps of weight loss are the pyrolysis of the organic ligand and/or the departure of the sulfate as SO_2 or SO_3; all are exothermic. For **1**·La and **6**·Eu, the residues above 800 °C have a composition of $Ln_2O_2SO_4$, and the observed residue percentages (and the theoretical values in parentheses) are 48.3 (48.1) and 46.2 (46.6) for **1**·La and **6**·Eu, respectively. $La_2O_2SO_4$ keeps stable and shows little change at the highest temperature, while $Eu_2O_2SO_4$ decomposes slowly from 1080 °C into Eu_2O_3 at the highest temperature. For **12**·Tm the residues above 800 °C might be a mixture of $Tm_2O_2SO_4$ and Tm_2O_3, decomposing completely to Tm_2O_3 from 1000 °C to the highest temperature.

The infrared spectra of complexes of the same type structure are very similar, while those of different structure types exhibit some difference. The difference between ν_{as}(COO) and ν_s(COO) bands are ca. 150, 140, and 130 cm^{-1} for type I, type III, and type II, agreeing with the fact that the carboxyl groups in types I and III are in bridging mode while in chelating mode in type II.[30] Four to six bands observed in range of 980−1270 cm^{-1} of sulfate ions (ν_1 and ν_3) indicates the lower symmetry of SO_4^{2-} ions, as the crystal structures revealed. The compounds belonging to different types possess different vibration bands of sulfate ion due to the distinct coordination modes of sulfate ion presenting in different types of structures. In addition, bands at ca. 3400 and 1600 cm^{-1} indicated the existence of coordination water in the structures.

(30) Nakamoto, K. *Infrared and Raman Spectra of Inorganic and Coordination Compounds*, Wiley: New York, 1986.

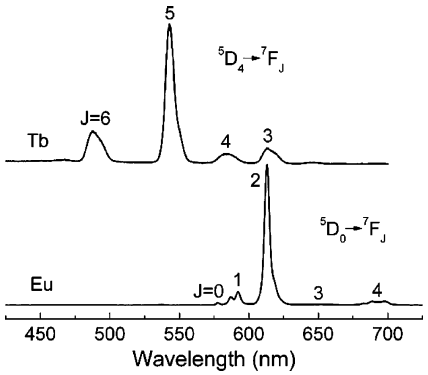

Figure 10. Luminescence spectrum of **6**·Eu and **8**·Tb at room temperature. Exciting light wavelengths are 315 and 303 nm, for **6**·Eu and **8**·Tb, respectively.

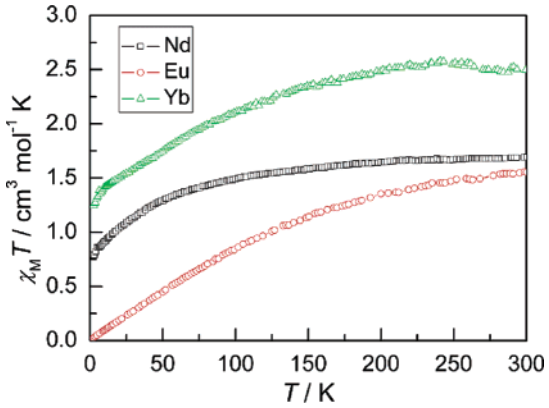

Figure 11. Temperature dependence of the $\chi_M T$ for **4**·Nd, **6**·Eu, and **13**·Yb at 1, 3, and 1 T, respectively.

The luminescence spectra of complex **6**·Eu and **8**·Tb at room temperature are shown in Figure 10. When excited at 315 nm, complex **6**·Eu exhibits very strong red luminescence, which arises from $^5D_0 \rightarrow {}^7F_J$ ($J = 0-4$) transitions, a typical characteristic of Eu^{3+}.[31] The main emission comes from the $^5D_0 \rightarrow {}^7F_2$ transition, which is induced by electric dipole moment and is hypersensitive to the environment of the Eu(III). Although the $^5D_0 \rightarrow {}^7F_1$ transition, which is a magnetic dipole transition and is fairly insensitive to the coordination environment of the Eu(III), is also present, it is 11 times less intense, indicating that the Eu(III) centers in **6**·Eu do not possess inversion symmetry.[32,33] This is in agreement with the result of the single-crystal X-ray analysis. Complex **8**·Tb emits green light when excited at 303 nm. The emission peaks at 488, 543, 585, and 613 nm can be assigned to $^5D_4 \rightarrow {}^7F_J$ ($J = 6, 5, 4, 3$) transitions, respectively.

Magnetic Properties. The temperature dependence of the magnetic susceptibility of **4**·Nd, **6**·Eu, and **13**·Yb is shown in Figure 11, where χ_M is the corrected molar magnetic susceptibility per Nd(III), Eu(II), and Yb(III) ion, respectively. The variation of $\chi_M T$ of **7**·Gd are shown in Figure 12, where χ_M is the corrected molar magnetic susceptibility per [Gd$_2$] binuclear unit.

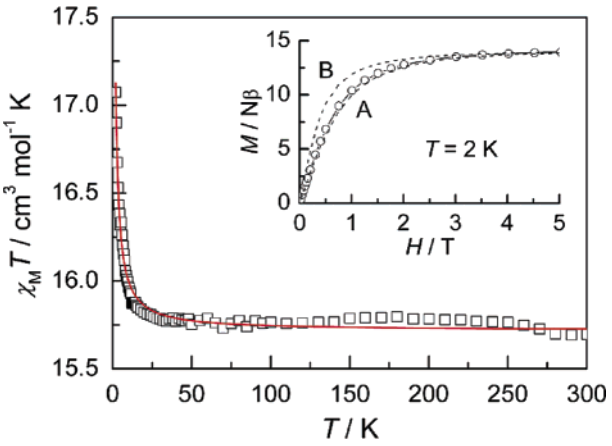

Figure 12. Temperature dependence of the $\chi_M T$ for **7**·Gd at 0.1 T. The red line is the theoretical curve obtained with $g = 2.0$ and $J = 0.024$ cm^{-1}. The inserted plot is the field-dependent magnetization of **7**·Gd at 2 K (circles). The dashed lines represent the Brillouin function for (A) two uncoupled Gd centers and (B) an $S = 7$ state.

The observed $\chi_M T$ of **4**·Nd at room temperature is 1.69 cm^3 mol^{-1} K, which is close to the theoretical value of 1.64 cm^3 mol^{-1} K for the free Nd(III) ion. On lowering the temperature, $\chi_M T$ continuously decreases to a value of 0.79 cm^3 mol^{-1} K at ca. 2.2 K. The thermal variation of $\chi_M T$ mainly depends on the populations of the Stark levels and on the possible magnetic interactions between Nd(III) ions. It is noted that the 4f^n configuration of a Ln(III) ion is split into $^{2S+1}L_J$ states by the interelectronic repulsion and the spin−orbit coupling. Further splitting into Stark components is caused by the crystal-field perturbation, which depends on the symmetry site of the ion.[32] At room temperature, all the Stark levels arising from the 10-fold degenerate $^4I_{9/2}$ ground states are populated, but as the temperature decreases, a progressive depopulation of these levels occurs.

For **5**·Eu, the observed $\chi_M T$ at room temperature is 1.56 cm^3 mol^{-1} K, slightly larger than the value 1.5 for a Eu(III) ion calculated by Van Vleck allowing for population of the excited state with higher values of J at 293 K. As the temperature is lowered, $\chi_M T$ decreases continuously, which should be attributed to the depopulation of the levels with nonzero J values. At the lowest temperature, $\chi_M T$ is close to zero, indicating a $J = 0$ ground state of the Eu(III) ion ($^7F_0$).

The thermal evolution of χ_M^{-1} of **7**·Gd obeys the Curie−Weiss law over the whole temperature range with a positive Weiss constant (θ) of 0.2 K and the Curie constant (C_M) of 15.74 cm^3 mol^{-1} K, which is consistent with the theoretical value for a binuclear complex of Gd (15.86 cm^3 mol^{-1} K).[34] It can be seen from Figure 12, at 300 K, that $\chi_M T$ is equal to 15.73 cm^3 mol^{-1} K; as the temperature is lowered, $\chi_M T$ remains almost constant to ca. 20 K and then increases rapidly on further cooling, reaching a maximum value of 17.07 cm^3 mol^{-1} K at 2 K. Such behavior can be referred to the presence of a weak ferromagnetic exchange behavior.

(31) Vicentini, G.; Zinner, L. B.; Zukerman-Schpector, J.; Zinner, K. *Coord. Chem. Rev.* **2000**, *196*, 353.
(32) (a) Bunzli, J.-C. G.; Chopin, G. R. *Lanthanide probes in Life, Chemical and Earth Sciences*; Elsevier: Amsterdam, 1989. (b) Costes, J.-P.; Nicodème, F. *Chem. Eur. J.* **2002**, *8*, 3442.
(33) (a) Judd, B. R. *Phys. Rev.* **1962**, *127*, 750. (b) Ofelt, G. S. *J. Chem. Phys.* **1962**, *37*, 511. (c) Blasse, G.; Grabmaier, B. C. *Luminescent Materials*; Springer-Verlag: New York, 1994.
(34) Lai, W. P. W.; Wong, W. T.; Li, B. K. F.; Cheah, K. W. *New J. Chem.* **2002**, *26*, 576.

The data have been quantitative analyzed on the basis of the equation[35] deduced from the isotropic spin Hamiltonian, $H = -JS_{Gd}S_{Gd'}$, with the quantum numbers $S_{Gd} = S_{Gd'} = 7/2$. The least-squares fit is given as a red line in Figure 12. The best-fit parameters are $J = 0.024$ cm^{-1} and $g = 2.0$ with an agreement factor R equal to 4.3×10^{-6} ($R = \Sigma[(\chi_M T)_{obs} - (\chi_M T)_{calc}]^2/\Sigma[(\chi_M T)_{obs}]^2$). The weak ferromagnetic nature of Gd···Gd interaction is further supported by the field-dependent magnetization at 2 K (Figure 11, inset). The line of experimental magnetization is comprised between the two dashed lines that correspond to two uncoupled Gd centers (A) and to a $S = 7$ state (B), which confirms the weak ferromagnetic interaction between the two Gd(III) ions. Such unexpected ferromagnetic behavior of **7**·Gd has been found in gadolinium complexes with a GdO_2Gd core, $[GdL_3(H_2O)]_2$ (HL = salicylic acid)[36a] ($J = 0.05$ cm^{-1}, $g = 2.0$) and $[Gd_2L_4(MeOH)_2(H_2O)_2]\cdot MeOH\cdot 2H_2O$ (HL = ferrocenecarboxylate)[36b] ($J = 0.006$ cm^{-1}, $g = 2.0$), in contrast with the most reported homopolynuclear gadolinium complexes which have antiferromagnetic ground states.[35,37] At this stage, the reason the two gadolinium ions present different magnetic interactions in different complexes with the same GdO_2Gd moiety is not clear yet.[36]

For **13**·Yb, $\chi_M T$ is equal to 2.50 cm^3 mol^{-1} K at room temperature, close to the theoretical value of 2.57 cm^3 mol^{-1} K for the free Yb(III) ion with a $^2F_{7/2}$ ground multiplet well-separated from excited ones, and decreases continuously to a value of 1.25 cm^3 mol^{-1} K at ca. 2.2 K. As in the case of **4**·Nd, the deviation of the magnetic susceptibility of **13**·Yb with respect to the Curie law should be mainly due to the temperature dependence of the population of the split Stark components, which arise from the ground multiplet under the crystal-field perturbation.[32a]

Conclusions

We have synthesized a new series of coordination polymers of the general formula $[Ln(INO)(H_2O)(SO_4)]_n$ (Ln = La−Lu) via hydrothermal reactions. These compounds crystallized in three new structural types: the La, Ce, Pr complexes exhibit a 3D pillared-layer structure (type I); the Nd, Sm, Eu, Gd, and Tb complexes show a 2-fold interpenetrated "3D herringbone" network (type II); and Ho, Er, Tm, Yb, and Lu complexes have a unique α-Po framework based on connected chains (type III). The progression from type I to type II and to type III with increasing atomic number is mainly ascribed to the effects of lanthanide contraction, which is reflected not only by the differences in bonding and nonbonding interatomic distances involving lanthanide ions but also by the differences in coordination number and geometry. Also interesting is the diverse coordination modes exhibited by the INO ligand and the sulfate ion. The versatile coordination ability of these bridging ligands makes them adaptable to lanthanide ions of different sizes and leads to the various topologies of the coordination networks.

Acknowledgment. We thank Prof. Song Gao and Mr. Haoling Sun for their kind help in magnetic measurement and valuable discussion. Financial support from NSFC (20221101, 20201009, 90201014, 20490210, and 20423005) and the Founder Foundation of PKU is gratefully acknowledged.

Supporting Information Available: An X-ray crystallographic file in CIF format of compounds **1**·La−**14**·Lu. This material is available free of charge via the Internet at http://pubs.acs.org.

IC0487575

(35) Panagiotopoulos, A.; Zafiropoulos, T. F.; Perlepes, S. P.; Bakalbassis, E.; Masson-Ramade, I.; Kahn, O.; Terzis, A.; Raptopoulou, C. P. *Inorg. Chem.* **1995**, *34*, 4918.

(36) (a) Costes, J.-P.; Clemente-Juan, J. M.; Dahan, F.; Nicodème, F.; Verelst, M. *Angew. Chem., Int. Ed.* **2002**, *41*, 323. (b) Hou, H.-W.; Li, G.; Li, L.-K.; Zhu, Y.; Meng, X.-R.; Fan, Y.-T. *Inorg. Chem.* **2003**, *42*, 428.

(37) (a) Liu, S.; Gelmini, L.; Rettig, S. J.; Thompson, R. C.; Orvig, C. *J. Am. Chem. Soc.* **1992**, *114*, 6081. (b) Hedinger, R.; Ghisletta, M.; Hegetschweiler, K.; Toth, E.; Merbach, A. E.; Sessoli, R.; Gatteschi, D.; Gramlich, V. *Inorg. Chem.* **1998**, *37*, 6698. (c) Costes, J. P.; Dahan, F.; Nicodème, F. *Inorg. Chem.* **2001**, *40*, 5285. (d) Costes, J.-P.; Dahan, F.; Dupuis, A.; Lagrave, S.; Laurent, J.-P. *Inorg. Chem.* **1998**, *37*, 153. (e) Costes, J.-P.; Dupuis, A.; Laurent, J.-P. *Inorg. Chim. Acta* **1998**, *268*, 125.